PREPRINT

CropQuant: An automated and scalable field phenotyping platform for crop monitoring and trait measurements to facilitate breeding and digital agriculture

Ji Zhou[1,2,*], Daniel Reynolds[1], Danny Websdale[1,3], Thomas Le Cornu[1], Oscar Gonzalez-Navarro[1,2], Clare Lister[2], Simon Orford[2], Stephen Laycock[3], Graham Finlayson[3], Tim Stitt[1], Matt Clark[1], Mike Bevan[2], Simon Griffiths[2,*]

[1]Earlham Institute, Norwich Research Park, Norwich UK
[2]John Innes Centre, Norwich Research Park, Norwich UK
[3]University of East Anglia, Norwich Research Park, Norwich UK
[*]Correspondence should be addressed to: ji.zhou@earlham.ac.uk & Simon.Griffiths@jic.ac.uk

Abstract

Automated field phenotyping provides continuous and precise measures of adaptation and performance traits that are key to today's breeding and agricultural practices. Besides monitoring morphological changes of crop growth and development, high-resolution and high-frequency of phenotypic measures can empower an accurate delineation of the genotype to phenotype pathway enabling the assessment of genes controlling yield potential and environmental adaptation. Here, we present CropQuant, a cost-effective Internet of Things (IoT) powered phenotyping platform, designed to be easily used and widely deployed in any environment. To manage and process data generated by the platform, we developed an automatic in-field control system, high-throughput trait analysis algorithms, and machine-learning based modelling to explore the dynamics between genotypes, phenotypes and environment. We used the platform in a 95-day field experiment to generate dynamic developmental profiles of five wheat genotypes within the single genetic background of *Paragon* (a UK spring wheat variety) and demonstrated a successful example of how this technology could be applied to breeding, crop research and digital agriculture.

NOTE: The final version of this manuscript provides much more detailed explanation of the CropQuant technology and novel biological discoveries through applying the field crop phenotyping technology in two-year wheat field experiments.

Background

The great American wheat breeder and Agri-Tech innovator Orville Vogel once stated that the plant you are looking for is in your plots, but you have to be there when it is. Four decades after temporary success in ensuring global food security, we are now facing an even bigger challenge to feed generations to come[1]. Due to a narrowing range of available genetic diversity of modern crop germplasm and increasing fluctuations in weather caused by global climate change[2], we rely on exploiting new sources of variation such as landraces and wild relatives to seek traits with greater yield potential as well as environmental adaptation[3]. This process requires robust measures of adaptive traits from many experimental plots throughout the growing season. Our work aims to address this challenge through a cost-effective IoT-powered phenotyping platform, **CropQuant**, which facilitates continuous monitoring and accurate measures of crop growth and development in different environments.

To increase yield and improve crop adaptation to diverse environments sustainably, modern genetic and genomics technologies have been employed to enable an efficient selection of valuable lines with high yield, biotic and abiotic stress tolerance, and disease resistance[3,4]. For example, QTL analysis and genome-wide association studies (GWAS) to examine genetic architecture[5], genome sequencing to reveal gene content and diversity[6] and marker-assisted selection (MAS) or genomic selection (GS) to accumulate favourable alleles[7]. However, these technical advances are limited by low-throughput, laborious and inaccurate in-field phenotyping approaches[8]. This is why phenotyping is widely recognised as the bottleneck that prevents us from linking the richness of genomic and genotypic information to important traits, so that they can be effectively deployed for agriculture.

To date, along with the development of remote sensing technologies[7] and open analytics software libraries[9], agricultural practitioners such as breeders, growers, farmers and crop scientists have been employing new approaches to relieve the bottleneck[10]. For instance, non-invasive remote sensors and aerial imaging devices such as unmanned aerial vehicles (UAV) and blimps are being used to study crop performance and field variability[11]. Satellite imaging[12] and tailored portable devices[13] are applied to the prediction of crop growth and yield potential based on canopy photosynthesis and normalised difference vegetation indices (NDVI). Large-scale imaging systems equipped with 3D laser scanners and multispectral sensors have been established to automate plant monitoring for a fixed number of pots or plots either in greenhouse (e.g. Scanalyzer HTS/3D HT, LemnaTec) or in the field (e.g. LeasyScan, Phenospex; Field Scanalyzer, LemnaTec)[14–16]. However, the challenges associated with these technologies are high costs, small scale, low frequency of measures and inadequate software analytical tools that can be used by agricultural practitioners to make sense of complicated phenotypic datasets[14,17]. From this perspective, our ability to measure crop growth dynamically and key adaptive traits in large numbers of experimental plots in different regions is still limited. Hence, there is a pressing need to develop an affordable and reliable phenotyping platform that can be easily used and widely adopted in breeding pipelines and by crop research communities worldwide.

The IoT-powered phenotyping platform

Here we describe the CropQuant platform designed to automatically monitor crop growth and development through low cost in-field terminal workstations. The current

design of the platform is driven by a number of IoT technologies[18], together with our vision for how to implement advanced Agri-Tech innovations in breeding, agriculture and crop research.

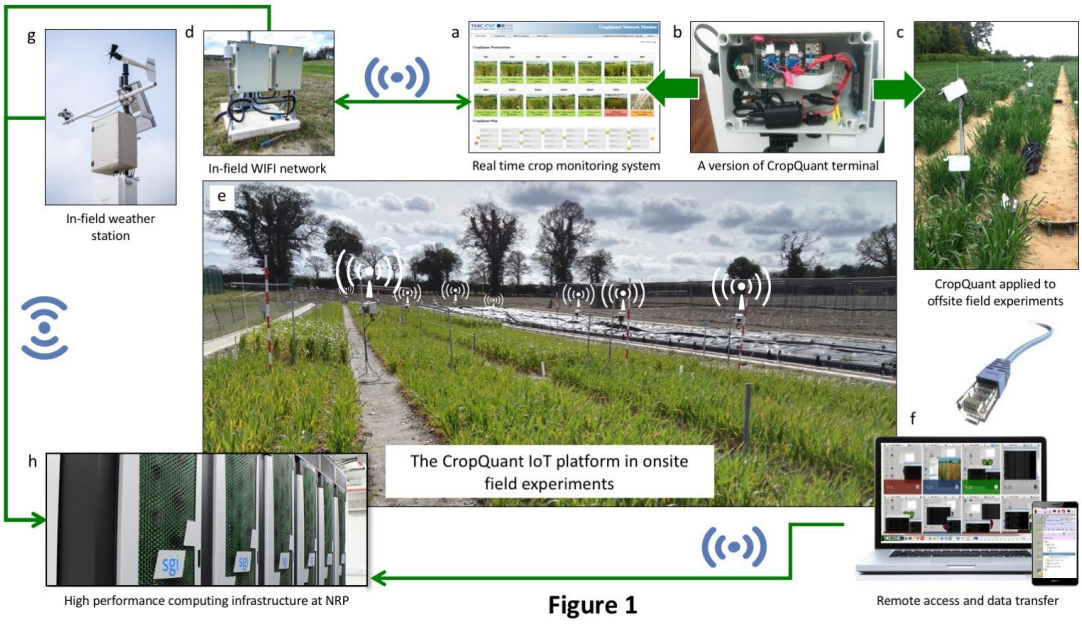

Figure 1. The CropQuant IoT platform in onsite and offsite field trials.
(**a**) CropMonitor, a centralised control system, administers CropQuant terminals and records online (green) or offline (red) status, operational mode (amber if imaging halts), daily images, micro-environment (e.g. temperature and humidity), and computational resource. (**b**) The hardware design of CropQuant terminals. (**c**) CropQuant used in offsite field trials, which was powered by batteries and solar panels. (**d**) An in-field WIFI system installed for onsite field trials. (**e**) The automated IoT platform established for onsite field trials. (**f**) Real-time crop monitoring through connecting CropQuant with a mobile device in the field or a computer in an office. (**g**) A comprehensive in-field weather station. (**h**) HPC is used for durable data storage and in-depth trait analysis.

Figure 1 shows an experimental scale CropQuant platform used in wheat in-field assessment plots, incorporating networked remote sensors, single-board computers, in-field wireless communication, and open data exchange solutions. There are 14 terminal workstations jointly operating on the platform, all of which are administered by a centralised control system called **CropMonitor** (**Fig. 1a** and **Supplementary Methods**). Using the platform, a number of tasks essential for next generation phenotyping[19] have been accomplished. They are *continuous monitoring* through high resolution time-lapse photography, *in-field evaluation* using dedicated hardware and software, and *efficient data transfer* via real-time file sharing and data exchange servers. To complete these tasks with low-cost hardware and minimal energy requirement, we have tested a range of single-board computers to conduct the above in-field computing tasks and chose to use *Raspberry Pi* 2, Pi camera modules (e.g. RGB, red/green/blue colour model), and remote sensor boards as the internal hardware (see **Final Publication**) due to the scalability and accessibility of the *Pi* computer. For the peripheral hardware, we have applied a weatherproof design to ensure environmental endurance, easy installation and outdoor maintenance (**Fig. 1b**

and **Final Publication**). A hardware list and a construction manual for CropQuant can be seen in **Final Publication.**

As onsite and offsite field experiments are conducted using diverse infrastructures, we produced two versions of CropQuant terminal. For offsite field experiments, a workstation is powered by a replaceable battery with trickle charging from a solar panel (**Fig. 1c**). It is self-operating during the growing season. We have implemented a headless access mode to enable high-speed data transfer and systems control via an Ethernet connection. For onsite field trials, CropQuant devices are powered by 5V/2A power supplies and connected to an in-field WIFI network acting as nodes in a mesh network (**Figs. 1d&e**, **Final Publication**). For both versions, we developed an open software package running on the Linux *Debian* operating system to enable image acquisition, image quality control, regular humidity/temperature recording, and systems interactions (**Supplementary Methods** and **Final Publication**).

The CropQuant platform facilitates automatic crop phenotyping. Scientists and agricultural practitioners can access every terminal workstation remotely for real-time monitoring, either using a mobile device (e.g. a tablet/smartphone) in the field or an office computer (**Fig. 1f** and **Final Publication**). They can inspect not only the whole field in different regions via CropQuant terminals, but also take control of any operational workstation to review the performance of crops, initiate new monitoring sessions, or transfer on-board phenotypic and sensor datasets to external computing storage. If users are granted administrative access to the platform, they can oversee the whole platform through CropMonitor, where the status of every terminal node is constantly updated by the control system, including information such as online and offline status, operational mode, representative daily images, micro-environment (e.g. temperature/humidity in a plot region), and computational resource such as CPU and memory (**Supplementary Methods** and **Final Publication**). The architecture of the control system supports the collation of phenotypic and sensor data for storage, visualisation, GUI-based systems interactions, and processing on high-performance computing (HPC) infrastructure (**Final Publication**).

As our long-term research interests lie in efficient gene discovery, crop adaptation, agronomic characterisation and crop management, we have installed a comprehensive in-field weather station for our onsite field trials. The station records a range of meteorological datasets including photosynthetically active solar radiation, rainfall, temperature, relative humidity and wind speed (**Fig. 1g**). Phenotypic and climate datasets are managed and saved in HPC (SGI UV 2000 system equipped with Intel Xeon cores) for durable data storage and centralised trait analysis (**Fig. 1h**).

The high-throughput analysis pipeline

We configured CropQuant terminals to carry out high-frequency (three times per hour) and high-resolution (2592x1944 pixels) of measurement to capture phenotypic plasticity, early expression of traits, and crop-environment interactions (**Final Publication**). For example, over 200 GB data have been generated by ten offsite CropQuant terminals in the 2015 field season, during a 95-day period. To extract meaningful results from the growth and developmental data effectively, we exploited some latest open-source analytic libraries such as OpenCV[20], Scikit-learn[21] and

Scikit-image[22] and developed automated bioimage informatics algorithms that are embedded in a high-throughput trait analysis pipeline.

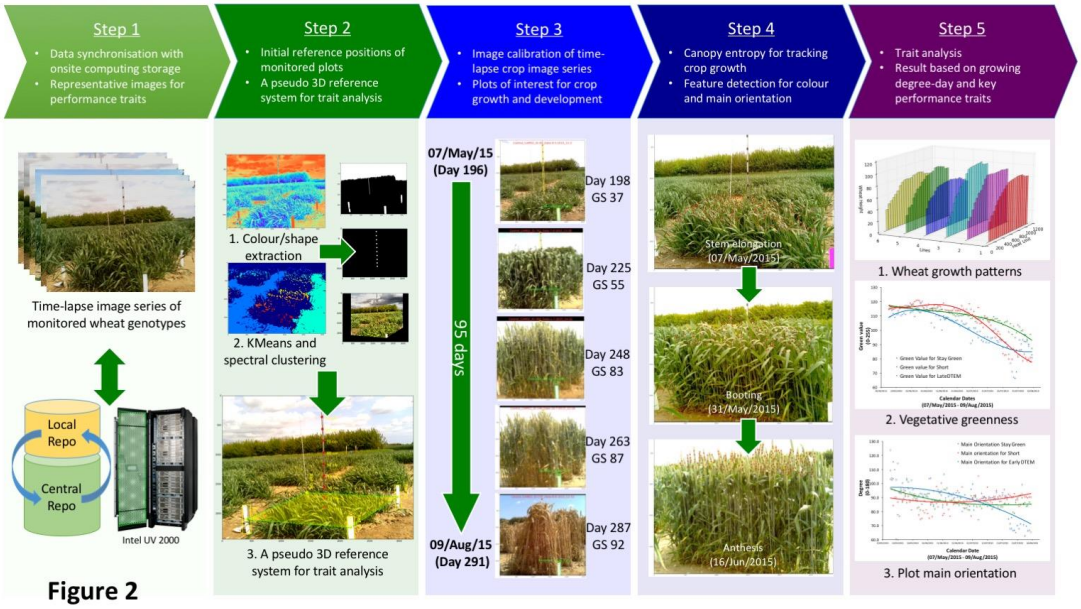

Figure 2. The high-throughput analysis pipeline for processing and quantifying crop growth patterns and adaptive traits.
In *step 1*, high-quality crop images are chosen by the selection algorithm and stored in both local and central Git repositories. In *step 2*, initial reference positions of five monitored plots are detected by the plot detection algorithm, which also calculates the pixel-metric conversion. In *step 3* and *4* of the pipeline, the CropMeasurer algorithm is used for tracking plots of interest based on the initial reference positions and then conducts in-depth traits analysis to measure the canopy region and key adaptive traits. In *step 5*, crop growth patterns in relation to thermal time (degree day), continuous vegetative greenness (0-255) and the change of the main orientation of given plots (0^{o}-180^{o}) are quantified and illustrated.

Figure 2 illustrates the analysis pipeline designed for both workstation computers and HPC. First, to arrange the collected crop images, we have developed a crop image selection algorithm to choose representative images according to their size, clarity, imaging dates and genotypes (**Fig. 2**, *Step 1*). Only high-quality images were retained for trait analysis (**Final Publication**). All datasets, including those low quality images, were stored in a central repository. Source code of the analysis pipeline was arranged into source trees and saved in both local and central Git repositories (**Supplementary Methods** and **Final Publication**).

Secondly, we have designed a detection algorithm to define reference positions of plots monitored during the experiment (**Fig. 2**, *Step 2*). In the real agricultural and breeding situations for which CropQuant was designed, strong wind, heavy rainfall, irrigation and chemical spraying will result some modest camera movements, which can cause issues when cross-referencing trait measures in a time-lapse image series. To resolve this issue, the algorithm identifies the initial reference position of a given plot and then geometrically transforms every image in the series to the same position for comparison. For instance, the algorithm detects coordinates of white reference canes (the plot region) and dark markers on a ranging pole (for crop height) using colour feature selection. Then, it classifies pixels into different groups such as crop

canopy, wheel tracks, and plot regions based on the machine-learning methods (e.g. k-means and spectral clustering). Finally, the algorithm establishes a pseudo reference system that records the plot area, the canopy space, height markers and the pixel-metric conversion (**Supplementary Methods** and **Final Publication**).

Following Step 2, we incorporated initial reference positions of monitored plots into the third algorithm called **CropMeasurer** for in-depth trait analysis. For a given genotype, CropMeasurer employs an adaptive intensity and gamma equalisation to adjust colour and contrast to minimise colour distortion caused by variable in-field lighting (**Supplementary Methods**). Then, the algorithm tracks geometric differences between the plot on a given image and the initial plot position. If different, a geometric transformation method is applied to recalibrate the image, which removes areas outside the plot area and could generate different sizes of black bars to the top of the given image (**Fig. 2**, *Step 3*). Within a given plot, CropMeasurer calculates the crop height by detecting the visible part of the ranging pole as well as the canopy region (**Final Publication**). Finally, the algorithm locates corner-featured points within the canopy region (**Fig. 2**, *Step 4*), which generates red pseudo points (**Supplementary Methods** and **Final Publication**) to represent the tips of erect leaves at stem elongation or jointing (the Zadoks scale[23], growth stages, GS 32-39), reflective surfaces of curving leaves and heads between booting and anthesis (GS 41-69), and corner-featured points on wheat spikes during senescence (GS 71-95).

In addition to crop growth patterns in relation to thermal time (degree day, ^{o}Cd), we have also included other dynamic measures of a number of traits in the pipeline (**Fig. 2**, *Step 5*). For example, vegetative greenness is calculated through separating the green channel in RGB images within plots of interest (**Supplementary Methods**). The output (0-255) has been used to assess green biomass and stay-green (prolonged green leaf area duration through delayed leaf senescence). Morphological traits such as the main orientation of a given plot (0^{o}-180^{o}) are quantified based on an optimised edge detection method, which computes the alignment of crop stems for assessing stem rigidity and lodging risk (**Supplementary Methods** and **Final Publication**).

Monitoring NILs of wheat using CropQuant

The radically different nature of environments where wheat is grown provides a unique opportunity to study the genetic diversity of wheat in connection with yield and stress tolerance through phenotypic differences[24]. Hence, we have chosen Near-isogenic lines (NILs) of wheat from our genetic stocks[25] to test the platform. Between May and August 2015, we monitored five NILs: Late-DTEM, days to ear emergence with *Ppd-1* loss of function (lof); Early-DTEM, *Ppd-D1a* photoperiod insensitivity; Short, *Rht-D1b* semi dwarfing; Stay-Green, a stay green induced mutant; and, *Paragon* wild type (WT). All NILs are in the genetic background of *Paragon* (a UK spring wheat variety) and were constantly monitored over a 95-day period (**Supplementary Methods** and **Final Publication**). **Figure 3a** illustrates dynamic developmental profiles of the five lines generated by CropQuant, together with environmental factors recorded during the period. Based on the developmental data, we computed daily relative growth rates (RGR) at different growth stages (**Fig. 3b**) and applied machine-learning based modelling to explore the dynamics between genotype, phenotype and environmental factors (**Figs. 3c-e**).

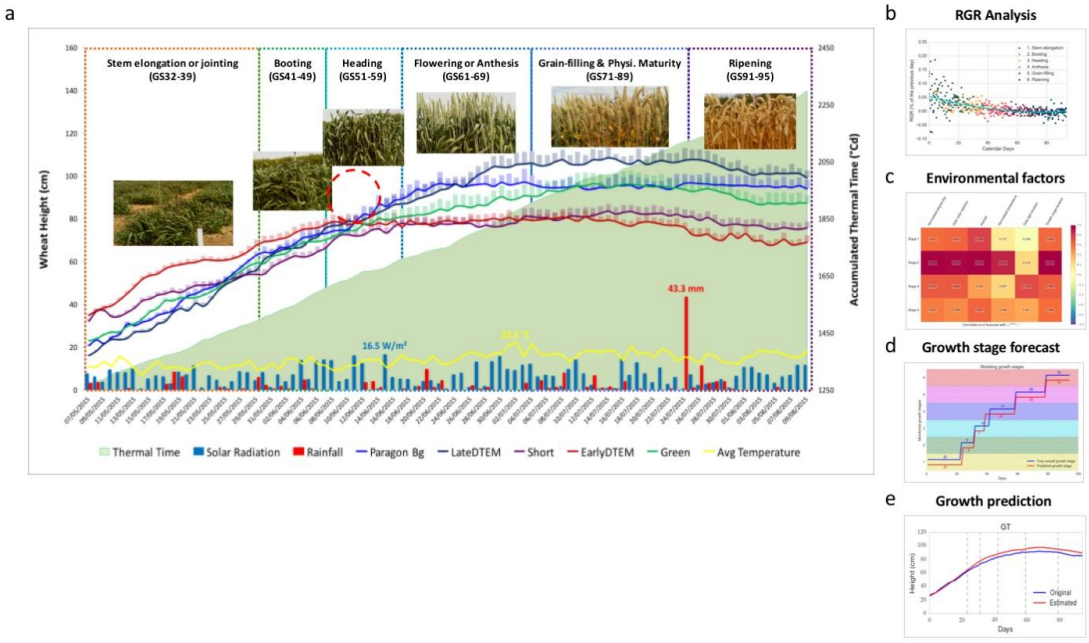

Figure 3

Figure 3. Monitoring wheat performance using the CropQuant platform and exploring the dynamics between genotype, phenotype and environment.
(**a**) Five NILs of wheat (Late-DTEM, Early-DTEM; Short, Stay-Green, and *Paragon* WT) and their performance in relation to environmental factors such as wind and rainfall, together with accumulated thermal time. Six growth stages of *Paragon* WT are used as reference. (**b**) RGR (growth % of the previous day) is used to present the daily growth rate of five NILs at different stages. (**c,d**) Both RGR and canopy height are responses of the correlation models that explore wheat growth and environmental factors, including thermal time, solar radiation, rainfall and the duration of growth stages, which are statistically significant using *Pearson* correlation ($p<0.01$). (**e**) A global wheat growth model comparing CropQuant growth measures. (**f**) A growth stages predictive model in comparison to manual phenotyping recording.

To measure the rate and sensitivity of wheat growth dynamically in relation to the environment, we used *Paragon* WT as the reference and highlight six key growth stages (GS32-95, **Fig. 3a**), from stem elongation or jointing (GS 32-39) to ripening (GS 91-95), the five growth curves generally followed a sigmoid curve. At the beginning of the crop monitoring, *Ppd-D1a* NIL was already at the end of the jointing stage (GS37-39) and hence was the first line reaching a maximum height. *Ppd-1* lof was the last to stop increasing in height. The heights of five NILs were very similar in the middle of June (highlighted by a red dash circle), which has verified what we had manually observed in the field as all the NILs were at different growth stages.

By cross-referencing five development profiles (based on growth stages, instead of calendar days), we notice that, although *Ppd-D1a* NIL and *Rht-D1b* were recorded at similar maximum heights (83.4cm and 80.6cm), the latter had a gentle-mannered growth pattern. It suggests that this line could be suitable for crop management as farmers and growers would have more time to decide whether to apply fertiliser and irrigation to assist the growth or to use chemical control to prevent rapid height increase[13]. *Ppd-1* lof's growth stages had been shifted back and thus had more time to develop. As a result, this line became the tallest in the trial. Although all five lines experienced some degree of height reduction due to a significant storm on 24th July 2015, *Paragon* WT presented a much lower lodging risk, as it maintained its height

during ripening (GS91-95). To verify the above observation, we have scored manually the heading dates and canopy height on the same plots and obtained a strong correlation (with correlation coefficient of 0.985, see **Final Publication**).

Moving beyond descriptive phenotypic research, we incorporated genotype (G), phenotype (P) and environmental (E) datasets into machine-learning based modelling to explore the dynamics between GxE. First, to understand which environmental factors were strongly correlated with the growth of the five NILs at every key growth stage, we computed daily RGR of the lines and associated the growth rate according with their growth stages. The scatter chart (**Fig. 3b**) shows the growth vigour of the five genotypes, active from jointing to flowering (GS32-69) and inactive after GS71 (grain-filling). After that, we calculated *Pearson* correlation coefficient and the p-value based on growth traits such as normalised RGR (nesting three-day rates to reduce noise) and canopy height at four key stages (i.e. jointing, booting, heading and flowering). Through this, we have identified six environmental factors that were significantly correlated with growth traits ($p < 0.01$) out of 14 (**Final Publication**). They are: normalised degree day, solar radiation, rainfall, normalised temperature, light duration, and growth stage duration. Two heat maps (**Figs. 3c** and **3d**) were produced to present the relationship between the identified environmental factors and two growth traits (RGR and canopy height) in relation to four key growth stages (GS32-69). As growth traits did *not* change excessively after anthesis (GS71-95), hence we did not include the later stages in the correlation analysis (**Supplementary Methods** and **Final Publication**).

Finally, using the six identified environmental factors and growth traits measured during the growing season, we explored a set of linear regression models to establish a global predictive model to forecast the growth and development of wheat in the genetic background of *Paragon*, when interacting with the environment. **Figure 3e** shows how the model forecasts the overall *Paragon* growth data (GT, mean squared error: 20.1512, correlation: 0.9991, **Supplementary Methods**). The model uses the six environmental factors at six stages (GS32-95) as the input to obtain estimates of the relative growth rates y_t for every given genotype (**Final Publication**). The formula $y_t = X_t^T * \beta_s + c$ was used for prediction, where X_t^T is the environmental data at a time point t, β is the model parameters for growth stage s, and c is a constant offset. We used ordinary least squares to determine the coefficients of the model. We also applied the model to predict the growth of the five NILs and compared the estimated growth with the recorded data generated by CropQuant (**Supplementary Methods** and **Final Publication**).

On the basis of the first predictive model, we produced a second model to forecast the timing and duration of key growth stages (GS32-95) to link the crop growth prediction with real-world agricultural practices. So, farmers, growers and breeders can make sound decisions based on the difference between the predicted growth curve and the actual growth pattern measured by CropQuant (**Final Publication**). This approach could also assist agricultural practitioners in terms of line selection, fertiliser application, irrigation and harvesting to secure yield production. **Figure 3f** illustrates the performance of the second model. It has employed a set of support vector machines (SVM) with radial basis function kernels to classify the timing and duration of key growth stages (**Supplementary Methods** and **Final Publication**). We tested

the model by comparing the predicted growth stages with the true data measured by crop physiologists (**Final Publication**).

Discussion

The CropQuant platform in combination with networked remote sensing, IoT in agriculture control systems, advanced bioimage informatics, and machine-learning based modelling is capable of relieving a major bottleneck in breeding, crop science and agriculture. The platform enables a future of easy-to-use field phenotyping in which real-time crop growth and development is now quantifiable. We made a viable model for IoT in agriculture, which can stretch the imagination of the Agri-Tech industry to seek cost-effective ways to increase the efficiency and accuracy for various agricultural practices. With more field trial data feeding into our GxE models from different regions around the world, we will improve our software solutions and models, so that we can assist agriculture professionals in making sensible decisions in their practices. To empower ease of use and wide adoption, we are continuously improving CropQuant hardware and software to promote our vision in Agri-Tech innovation, including *mobility* (easy to install and use), *capability* (real-time in-field analysis), *affordability* (competitive costs) and *durability* (long-lasting in the field conditions).

Methods

Methods and any associated references are available in the online version of the paper.

Note: Supplementary information is available in the final published version of the paper.

Author contributions

J.Z, D.R., S.L., T.S., M.C., M.B. and S.G. designed research; J.Z., D.R., O.G., C.L. and S.O. performed research; J.Z., D.R., T.C. and D.W. contributed hardware design and the development of analytics software; J.Z., D.R., T.C., D.W., O.G., C.L. M.B. and S.G. analysed data; and J.Z., D.R., T.C., D.W. and S.G. wrote the paper. All authors have read and approved the final manuscript

Competing financial interests

The authors declare no competing financial interests.

References

1. Pingali, P. Green Revolution:Impacts, Limits, and the path ahead. *Proc. Natl. Acad. Sci.* **109,** 12302–12308 (2012).
2. McCouch, S. *et al.* Agriculture: Feeding the future. *Nature* **499,** 23–24 (2013).
3. Tester, M. & Langridge, P. Breeding Technologies to Increase Crop Production in a Changing World. *Science.* **327,** 818–822 (2010).
4. Shrestha, R. *et al.* Bridging the phenotypic and genetic data useful for integrated breeding through a data annotation using the Crop Ontology developed by the crop communities of practice. *Front. Physiol.* **3,** 326 (2012).
5. Yang, W. *et al.* Combining high-throughput phenotyping and genome-wide association studies to reveal natural genetic variation in rice. *Nat. Commun.* **5,** 1–9 (2014).
6. Brenchley, R. *et al.* Analysis of the bread wheat genome using whole-genome shotgun sequencing. *Nature* **491,** 705–10 (2012).
7. Araus, J. L. & Cairns, J. E. Field high-throughput phenotyping: the new crop breeding frontier. *Trends Plant Sci.* **19,** 52–61 (2014).
8. Furbank, R. T. & Tester, M. Phenomics--technologies to relieve the phenotyping bottleneck. *Trends Plant Sci.* **16,** 635–44 (2011).
9. Eliceiri, K. *et al.* Biological imaging software tools. *Nat. Methods* **9,** 697–710 (2012).
10. Houle, D., Govindaraju, D. R. & Omholt, S. Phenomics: the next challenge. *Nat. Rev. Genet.* **11,** 855–866 (2010).
11. Sankaran, S. *et al.* Low-altitude, high-resolution aerial imaging systems for row and field crop phenotyping: A review. *Eur. J. Agron.* **70,** 112–123 (2015).
12. Zaman-Allah, M. *et al.* Unmanned aerial platform-based multi-spectral imaging for field phenotyping of maize. *Plant Methods* **11,** 35 (2015).
13. Pask, A., Pietragalla, J. & Mullan, D. *Physiological Breeding II: A Field Guide to Wheat Phenotyping*. *CIMMYT* (CIMMYT, 2012). doi:10.1017/CBO9781107415324.004
14. Barabaschi, D. *et al.* Next generation breeding. *Plant Sci.* **242,** 3–13 (2015).
15. Vadez, V. *et al.* LeasyScan: A novel concept combining 3D imaging and lysimetry for high-throughput phenotyping of traits controlling plant water budget. *J. Exp. Bot.* **66,** 5581–5593 (2015).
16. Karp, A. *et al.* Growing innovations for the bioeconomy. *Nat. Plants* **1,** 15193 (2015).
17. White, J. W. *et al.* Field-based phenomics for plant genetics research. *F. Crop. Res.* **133,** 101–112 (2012).
18. Gubbi, J., *et al*. Internet of Things (IoT): A Vision, Architectural Elements, and Future Directions. *Futur. Gener. Comput. Syst.* **29,** 1645–1660 (2013).
19. Cobb, J. N., *et al*. Next-generation phenotyping: Requirements and strategies for enhancing our understanding of genotype-phenotype relationships and its relevance to crop improvement. *Theor. Appl. Genet.* **126,** 867–887 (2013).
20. Howse, J. *OpenCV Computer Vision with Python*. (Packt Publishing Ltd., 2013). at <www.it-ebooks.info>
21. Pedregosa, F. *et al.* Scikit-learn: Machine Learning in Python. *J. Mach. Learn. Res.* **12,** 2825–2830 (2011).
22. van der Walt, S. *et al.* Scikit-image: image processing in Python. *PeerJ* **2,** 1–18 (2014).
23. ZADOKS, J. C., CHANG, T. T. & KONZAK, C. F. A decimal code for the

growth stages of cereals. *Weed Res.* **14,** 415–421 (1974).

24. Semenov, M. A. & Doblas-Reyes, F. J. Utility of dynamical seasonal forecasts in predicting crop yield. *Clim. Res.* **34,** 71–81 (2007).

25. Griffiths, S. *et al.* Meta-QTL analysis of the genetic control of ear emergence in elite European winter wheat germplasm. *Theor. Appl. Genet.* **119,** 383–95 (2009).

Supplementary Methods

Five wheat NILs used in the field trial represent a range of genetic variation all with the genetic background of the UK elite spring wheat '*Paragon*'. The development of the Late-DTEM: Par (Norstar + Gamma 319c) 3c-11, *Ppd-1* loss of function (lof) lines is described previously[26]. The development of the Early-DTEM NILs: Par (GS100 2A+CS2B+Son64 2D)-T10 B10 -3b16 and *Ppd-D1a* photoperiod insensitive has also been published[27]. The novel line Stay-Green is line 2316b selected on the basis of stay green phenotype from a population of 7000 *Paragon* EMS mutants carried through single seed descent up to M6 developed under the Wheat Genetic Improvement Network of the UK Department of Food and Rural Affairs (Defra). The semi-dwarf NILs (short) were produced by marker assisted backcrossing (to BC6) using *Rht-B1* and *Rht-D1* KASP markers (LGC). which is available online from http://www.cerealsdb.uk.net/cerealgenomics/CerealsDB. The sources of *Rht-D1b* and *Rht-B1b* were the UK winter wheat varieties 'Alchemy' and 'Robigus' respectively. The five wheat lines were sown in single 1 m^2 plots in autumn 2014 at Church Farm, Norfolk UK, and grown according to standard agronomic practice. The manual score of the date for ear emergence (DTEM) was done when 50% of the plot showed 50% emergence of the ear from the flag leaf. The manual measurement of plant height was done from the ear tip to ground level.

The CropQuant hardware contains many components. The centre one of the design is a *Raspberry Pi* 2 or *Pi* 3 single-board computer (we are also testing Intel® Edison in the new version of CropQuant). Based on a mobile ARM processor, the *Raspberry Pi* computer features on-board external connections in the form of USB and Ethernet to allow expansion using additional peripherals as well as an array of digital GPIO pins to interface with. The crop growth image acquisition was performed using a 5MP RGB or NoIR (No Infrared, for night vision) camera module connected via a CSI port on the *Pi* mother board. Digital temperature and humidity sensors are connected via manufacturer supplied circuits to the GPIO pins of the *Pi* for interactive control. The sensors themselves are mounted separate from the circuits, externally on the CropQuant's housing, wired through the base of the device and sheltered by a smaller, open housing unit. The external mounting allows for accurate sensing of ambient air conditions while sheltering the electronics from direct water damage. The CropQuant terminal is housed within a weatherproof (IP66 rated) plastic container, sealed around all openings allowing operation in the field conditions. Physical connection to the system for data transfer via USB or Ethernet and power (12/5V DC) is facilitated by water-resistant couplers designed to be sealed against the rain and air moisture.

The CropQuant software package runs on Linux-based operating system *Debian*. It contains two servers, NetATalk and VNC sever, to facilitate in-field data transfer and remote systems control, which allows users to connect to every CropQuant terminal through a wireless (using a tablet or a smartphone) or a wired connection (using a laptop). To enable real-time systems interactions, a GUI-based imaging program has been developed and added into the software package to control the RGB or NoIR camera module for time-lapse crop monitoring. The program can automatically detect the IP address of a given CropQuant terminal to associate the terminal with its specific experiment ID of the field trial. After that, the program requests users to specify information such as genotype, biological replicates and imaging duration via a

GUI dialog box, where users can initiate the image acquisition. The program can automatically adjust white balance, exposure mode and shutter speed in relation to variable in-field lighting conditions using the *picamera* package, a pure Python interface to the *Raspberry Pi* camera hardware. Both image resolution and imaging frequency (three times per hour in our field trials) can be changed if users want to modify their experimental settings. The program also conducts the initial quality control and data backup after every image is captured. The GUI-based imaging script is freely available for download at (see final publication).

Besides the image acquisition, the software package also contains functions such as synchronising with the central server twice within an hour to upload sensor data and CropQuant hardware information (see CropMonitor). Representative daily images are routinely selected and transferred to the central server during the night, which provides a daily snapshot of the monitored crops. Relying on the *crontab* scheduling system, we can monitor the performance of the software package and resume it automatically in cases of software interruption or power disruption. The SD card image running on the current version of CropQuant workstations can be downloaded via (see final publication).

CropMonitor is the next-generation IoT control system developed to oversee the field trial. It is performed using a central web server, logging updates received from individual clients, CropQuant terminals. A Python application on each workstation is run at regular intervals, scheduled by the native Unix *Cron* system. The application queries the terminal to determine workstation status information such as uptime, network addresses and storage usage. Sensor data and more variable system data such as CPU temperature and processor/memory usage is sampled at a higher frequency and a mean average of the readings is recorded during the query. Once the application has collected all necessary data it is encoded into a JSON data object and transmitted over HTTP to the central server which stores the data in an SQL database running on HPC. CropQuant status is displayed and automatically updated using a web-based interface, determining whether each node is online by the time of their last update. The web interface provides information, including the location of every CropQuant in the field (a field map needs to be uploaded to the central server), graphs of collected terminal/sensor data, and facilitates SSH and VNC linking to all active nodes. The CropMonitor system provides a centralised real-time monitoring system to administer the network of in-field workstations and collate collected data for visualisation, batch processing and annotation.

The image selection algorithm is designed to perform speedy assessment of large image datasets captured in field trials by comparing images to a number of fixed criteria. The Python-based algorithm can be executed either on a normal computer or HPC. All images which meet the analysis standards will be collated. In turn, each image is quantified by brightness, shadow percentage and sharpness, allowing all images which perform above a set of thresholds to be retained for further traits analysis. To determine the brightness of an image, the median value of pixel intensity is taken by transforming the image into HSV colour space. If the median intensity value is lower than a set threshold, the image is culled and not used from this point forward. The image clarity is determined by applying a Sobel edge detection[28] to the image. The detectable edges are calculated and then correlated with sharpness and exposure range of the image. The result of the clarity detection is also compared to a

set threshold, which will disqualify images if they are out of focus or unclear with ill-defined edges. The final image test is of the percentage shadow within the visible area. Dark pixels found in an image with an illumination value of below 20% are either too dark for feature extraction or containing too much shadow in the monitored plots. Once all comparisons have been passed, selected images are included in a result folder with a CSV file recording image metadata for further high-throughput image analysis. The iPython notebook of the image selection algorithm is freely available at (see final publication).

The plot detection algorithm detects initial reference positions of monitored plots. The algorithm identifies the coordinates of white reference canes (the plot region) and dark height markers on a ranging pole using colour-based feature selection on the basis of HSV (hue, saturation and value) and *Lab* non-linear colour space. It also classifies pixels into different groups such as sky, soil between plots, crop canopy, shadow, and plot regions using unsupervised machine-learning techniques such as K-Means[29] and spectral clustering[30]. After detecting initial reference objects in the image, the algorithm establishes a pseudo 3D reference system that records the 2D coordinates of the plot area, the canopy region, and height markers through a range of feature selection approaches. The pixel-metric conversion is also computed based on height markers on the ranging pole. The iPython notebook of the crop plot detection algorithm is freely available at (see final publication).

The CropMeasurer algorithm employs an adaptive intensity and dynamic gamma equalisation[31] to adjust colour and contrast to minimise colour distortion caused by diverse in-field lighting. Then, the algorithm tracks geometric differences between the plot on a given image and the initial position. If different, a geometric transformation method[32] will be applied to recalibrate the image, which removes areas outside the plot area and could generate different sizes of black bars to the top of the given image. Within a plot, CropMeasurer tracks the crop height by detecting the visible part of the ranging pole and defines the canopy region through a combined adaptive thresholding and local Otsu threshold methods[33]. Finally, the algorithm applies Harris and Shi-Tomasi corner detection methods[34] to locate corner-featured points within the canopy region. Red pseudo points are generated to represent the tips of erect leaves, reflective surfaces of curving leaves, heads and the corner points on ears. The main orientation of a given plot is quantified based on an optimised Canny edge detection method[35], which computes the alignment of crop stems. The iPython notebook of the image selection algorithm is freely available for download at (see final publication).

Data interpolation and analysis have been used to handle minor data loss during the field experiments. Four days' data gap (at the end of May 2015) has been recorded on a number of offsite CropQuant workstations, which was caused by SD card crash due to short-term power failure. We therefore used cubic spline interpolation method[36] to fill the gap in the phenotypic datasets.

The GxPxE interaction model explores the interactions between the recorded crop growth of five wheat genotypes and a number of environmental factors. Correlations are performed for each environmental factor grouped over three days with the recorded growth data. The reason to group environmental factors into nested three-day periods is to remove outliers and smooth the input data. The correlations are determined for each growth stage for five genotypes. The analysis is performed on the

grouped data as particular stages (e.g. booting and heading) contain few recorded growth data due to the short duration of both stages were present during the growth. To obtain he dynamic between relative growth rates (RGR) and environmental factors, we used the formula $(e^{RGR})^{-1}$ to transfer negative correlation values, as the RGR series is a decreasing sequence in relation to the increasing nature of growth stages.

Based on significant environmental factors, a set of linear regression models[32] have been explored and a single linear regression model is selected to estimate RGR of five genotypes in relation to given in-field environment conditions. Environmental factors with insignificant correlations (where $p > 0.01$, with respect to the height over the entire time-series) are removed from the analysis as they provide little predictive power. Ordinary least squares are used to derive the model coefficients and all the stages are included as features. The RGR data is normalised to present percentage changes in height between two consecutive days. To predict the canopy height for a given genotype, environment data at each growth stage is input to the global model. To derive the height of the plant over time, successive applications $h_t = h_{t-l}(1 + y_t)$ are applied, where h_t is taken from the above equation, h_{t-l} is the height of the plant at the previous time-point, and h_0 is equal to the initial height.

The performance of the model is verified by estimating the growth of all five NILs, including the overall paragon growth data (GT). The estimation is displayed with respect to the true canopy height datasets. The mean squared error recorded for G2 (*genotype two*, Late-DTEM), G3 (*genotype three*, Early-DTEM) and G4 (*genotype four*, Stay-Green) shows that the estimated height is close to the true growth curves. However, the error is much larger for G1 (*genotype one*, *Paragon* WT) and G5 (*genotype five* Short). This is due to the majority of crop growth happens during the early stages (GS32-GS59), estimation deviation during these initial stages could affect the overall height results. As the global predictive model might not be sensitive towards specific genotypes, we are still seeking a better approach to incorporate all genotypes with a similar genetic background into the prediction. The iPython notebook of the **GxPxE** interaction model can be downloaded at (see final publication).

The growth stage predictive model is based on the GxPxE model described before. The model is produced to explore how to predict growth stages of different wheat genotypes on the basis of real growth traits and environment data. It employs support vector machines (SVM)[34] with radial basis function kernels to classify growth stages, as SVMs are popular machine learning techniques for classification. The performance of the model is tested by overall paragon wheat growth data (GT) and *Paragon* WT (G1), as GT performs well in the GxPxE interaction model whereas G1 performs poorly. The prediction in comparison with the manually recorded growth stages suggests a successful prediction of the timing and duration of stem elongation and jointing (GS32-39) through heading (GS51-59) and flowering (GS61-69) through Ripening (GS91-95). However, the transition from heading to flowering has introduced an error, the transition has been predicted three days earlier. The main reason for this error is due to the short duration of booting (GS41-49) and heading (GS51-59). All genotypes used for training cannot sufficiently differentiate the two stages. For this matter, we are planning to add more training datasets from other varieties such as Watkins and Chinese Spring wheat in other field trials. As the model can be used to classify growth stages with real in-field data, we have made the model

623 freely available for other crop research groups to verity as well as jointly improve.
624 The iPython notebook of the growth stage model can be downloaded at (see final
625 publication).
626
627 **All supplementary movies** mentioned in the manuscript can be freely downloaded at
628 (see final publication)

Online methods references

26. Shaw, L. M., Turner, A. S., Herry, L., Griffiths, S. & Laurie, D. A. Mutant alleles of Photoperiod-1 in Wheat (Triticum aestivum L.) that confer a late flowering phenotype in long days. *PLoS One* **8,** (2013).
27. Shaw, L. M., Turner, A. S. & Laurie, D. A. The impact of photoperiod insensitive Ppd-1a mutations on the photoperiod pathway across the three genomes of hexaploid wheat (Triticum aestivum). *Plant J.* **71,** 71–84 (2012).
28. Szeliski, R. *Computer Vision : Algorithms and Applications*. (Springer Science & Business Media, 2010). doi:10.1007/978-1-84882-935-0
29. Aloise, D., Deshpande, A., Hansen, P. & Popat, P. NP-hardness of Euclidean sum-of-squares clustering. Mach. Learn. 75, 245–248 (2009).
30. Shi, J. & Malik, J. Normalized cuts and image segmentation. IEEE Trans. Pattern Anal. Mach. Intell. 22, 888–905 (2000).
31. Bassiou, N. & Kotropoulos, C. Color image histogram equalization by absolute discounting back-off. Comput. Vis. Image Underst. 107, 108–122 (2007).
32. Sezgin, M. & Sankur, B. Survey over image thresholding techniques and quantitative performance evaluation. J. Electron. Imaging 13, 146–165 (2004).
33. Otsu, N. A threshold selection method from gray-level histograms. IEEE Trans. Sys, Man and Cyber. 9, 62-66 (1979).
34. Harris, C. & Stephens, M. A Combined Corner and Edge Detector. Procedings Alvey Vis. Conf. 1988 147–151 (1988).
35. Kimmel, R. & Bruckstein, A. M. Regularized Laplacian zero crossings as optimal edge integrators. Int. J. Comput. Vis. 53, 225–243 (2003).
36. R Development Core Team. *R : A Language and Environment for Statistical Computing*. **1,** (R Foundation for Statistical Computing, 2008).
37. Montgomery, C., et al. Introduction to linear regression analysis. John Wiley & Sons, 2015.
38. Hsu, C.-W. & Lin, C.-J. A comparison of methods for multiclass support vector machines. *IEEE Trans. Neural Networks* **13,** 415–425 (2002).